Lipid Membranes Modulate the Structure of Islet Amyloid Polypeptide[†]

Sajith A. Jayasinghe and Ralf Langen*

Department of Biochemistry and Molecular Biology, Zilkha Neurogenetic Institute, University of Southern California, 1501 San Pablo Street, Los Angeles, California 90033

Received May 5, 2005; Revised Manuscript Received June 22, 2005

ABSTRACT: The 37-residue islet amyloid polypeptide (IAPP) is thought to play an important role in the pathogenesis of type II diabetes. Despite a growing body of evidence implicating membrane interaction in IAPP toxicity, the membrane-bound form has not yet been well characterized. Here we used circular dichroism (CD) and fluorescence spectroscopy to investigate the molecular details of the interaction of IAPP with lipid membranes of varying composition. In the presence of membranes containing negatively charged phosphatidylserine (PS), we observed significant acceleration in the formation of IAPP aggregates. This acceleration is strongly modulated by the PS concentration and ionic strength, and is also observed at physiologically relevant PS concentrations. CD spectra of IAPP obtained immediately after the addition of membranes containing PS revealed features characteristic of an α-helical conformation approximately ∼15−19 residues in length. After a longer incubation with membranes, IAPP gave rise to CD spectra characteristic of a *β*-sheet conformation. Taken together, our CD and fluorescence data indicate that conditions that promote weakly stable α-helical conformations may promote IAPP aggregation. The potential roles of IAPP−membrane interaction and the novel membrane-bound α-helical conformation in IAPP aggregation are discussed.

The deposition of proteins as amyloid fibrils is a characteristic feature of many human diseases, including Alzheimer's disease, Parkinson's disease, the prion-related transmissible spongiform encephalopathies (*1*), and non-insulin-dependent type II diabetes (*2*). Although there appears to be little or no sequence homology between the proteins involved in amyloid disease, a growing body of evidence suggests that fibril formation may follow similar pathways (*1*). Amyloid fibril formation is a nucleation-dependent, multistep process, in which the formation of numerous small oligomeric assemblies of proteins is thought to precede the formation of mature fibrils. Whether oligomers or mature fibrils are toxic and responsible for disease pathogenesis remains an active area of investigation.

It has been shown that several amyloidogenic proteins interact with lipid membranes, and it has become increasingly recognized that membrane interaction may well be involved in the pathogenesis of amyloid disease. Membranes have been implicated both as the targets of toxicity, via membrane disruption, and as the catalysts that facilitate protein aggregation (*3*−*18*).

Amyloid deposits and aggregates of the 37-residue IAPP[1] are thought to play an important role in non-insulin-dependent type II diabetes. A significant number of patients with this disease show IAPP amyloid deposits associated with areas of pancreatic *β*-cell dysfunction and death (*2*, *19*). Characterization of mature IAPP fibrils has revealed structural features that are typical of amyloid fibrils. IAPP fibrils contain a significant amount of *β*-sheet structure (*20*, *21*); their peptide chains are arranged in a cross-*β*-configuration wherein individual *β*-strands are arranged perpendicular to the fibril axis (*22*). Electron paramagnetic resonance data suggest a parallel arrangement of IAPP monomers within the fibril (*23*) similar to that of other amyloid fibrils (*24*−*26*). Furthermore, IAPP has been found to form voltage-dependent ion selective pores in planar lipid bilayers (*27*), to mediate vesicle aggregation (*28*), and to induce leakage of lipid vesicle contents by a "porelike" mechanism (*29*). Finally, a recent report has detailed the ability of lipid membranes containing phosphatidylglycerol to accelerate the kinetics of IAPP fibrillization (*30*), although the molecular mechanism of such an acceleration remains unknown.

In this study, we sought to characterize the interaction of IAPP with lipid membranes through the use of CD and fluorescence spectroscopy. We found, in agreement with previous studies, that membranes containing negatively charged lipids significantly modulate the kinetics of IAPP aggregation. This aggregation was modulated by the membrane PS concentration as well as the buffer ionic strength. Notably, we observed significant acceleration even at physiologically relevant PS and salt concentrations. Aggregation of IAPP in the presence of membranes is accompanied by an α-helical to *β*-sheet conformational reorganization. Our data suggests that conditions promoting a weakly stable α-helical conformation can accelerate IAPP aggregation.

EXPERIMENTAL PROCEDURES

Materials. Hexafluoro-2-propanol (HFIP) and ThT were obtained from Sigma-Aldrich (Milwaukee, WI). 1-Palmitoyl-2-oleoyl-*sn*-glycero-3-phosphatidylcholine and 1-palmitoyl-

[†] This work was supported by the Beckman Foundation and the Pew Scholars Program in the Biomedical Sciences (to R.L.).

* To whom correspondence should be addressed. Phone: (323) 442-1323. Fax: (323) 442-4404. E-mail: langen@usc.edu.

[1] Abbreviations: IAPP, islet amyloid polypeptide; PS, phosphatidylserine; CD, circular dichroism; EM, electron microscopy; ThT, thioflavin T; HFIP, hexafluoro-2-propanol; A*β*, amyloid *β*.

10.1021/bi050840w CCC: $30.25
Published on Web 08/17/2005

2-oleoyl-*sn*-glycero-3-[phospho-L-serine] were obtained as solutions in chloroform from Avanti Polar Lipids Inc. (Alabaster, AL). Synthetic wild-type human (h-IAPP) and rat IAPP (r-IAPP) were obtained from Bachem (King of Prussia, PA).

Preparation of Peptide Stock Solutions. Lyophilized IAPP peptides from Bachem were dissolved in HFIP to obtain clear solutions. Peptide concentrations were calculated by UV absorbance at 280 nm in 6 M guanidine HCl, using an extinction coefficient of 1400 M^{-1} cm^{-1}. Stock solutions in HFIP were stored at −70 °C.

Preparation of Large Unilamellar Vesicles (LUV). To obtain the desired phosphatidylcholine to PS molar ratios, appropriate amounts of lipid solutions in chloroform were mixed; the chloroform was evaporated under a stream of nitrogen and dried in a vacuum desiccator overnight. The dry lipid films were rehydrated in the appropriate buffer, subjected to five freeze−thaw cycles, and extruded using a mini-extruder fitted with 0.1 nm polycarbonate membranes (Avanti Polar Lipids Inc.) to produce LUV with a diameter of 100 nm.

CD Spectroscopy. Aliquots of peptide stock solutions in HFIP were pipetted into 1.5 mL Eppendorf tubes, mixed with 500 μL of deionized distilled water, immediately frozen in liquid nitrogen, and lyophilized overnight. Dry lyophilized peptide was dissolved in the appropriate buffer to yield 25 μM solutions prior to use, and transferred into a 1 or 2 mm path length quartz cell. CD spectra were obtained using a Jasco 815 spectropolarimeter (Jasco Inc., Easton, MD). Measurements were taken every 0.5 nm at a scan rate of 50 nm/min, with an averaging time of 1 s. All spectra were corrected using appropriate backgrounds. Data were collected between 190 and 260 nm. Typically, two scans were averaged for peptides in the presence of LUV to minimize the contribution from multiple conformations due to aggregation. Background spectra were obtained by averaging 50 scans.

The fraction of helicity, $f_{\alpha H}$, for IAPP in an α-helical conformation was estimated using the equation $f_{\alpha H} = (\Theta_{obs} - \Theta_{RC})/(\Theta_H - \Theta_{RC})$, where Θ_{obs} is the observed ellipticity and Θ_{RC} and Θ_H are the ellipticity values for a completely random and completely helical peptide with a length equal to that of IAPP, respectively (*31*). Values for Θ_H (-34.7×10^3 deg cm^2 $dmol^{-1}$) and Θ_{RC} (895 deg cm^2 $dmol^{-1}$) were calculated as described in the literature (*31*, *32*). All ellipticity values were at 222 nm. The measured ellipticity (θ, millidegrees) was converted to the mean residue molar ellipticity (Θ, deg cm^2 $dmol^{-1}$) using the relation $\Theta = \theta/nCl$, where n represents the number of residues in IAPP, C the molar concentration, and l the path length of the cuvette in millimeters.

ThT Fluorescence Assay. Fibrillization of IAPP was monitored using the fluorescence intensity increase for ThT, a dye commonly used to detect protein aggregation. IAPP solutions for the ThT fibrillization assay were prepared as described for CD spectroscopy. To each fibrillization reaction mixture was added a sufficient amount of ThT to yield a 25 μM solution (from a 5 mM stock solution in deionized distilled water) immediately after the peptide had been dissolved in buffer, and real-time emission intensities were measured at 482 nm with excitation at 450 nm. Measurements were performed at room temperature with excitation and emission slit widths of 1 and 10 nm, respectively. Fluorescence measurements were taken using a Jasco FP-6500 spectrofluorometer.

Plots of ThT emission intensity as a function of time were fitted to a sigmoidal curve with the equation $I = I_i + m_i t + ((I_f + m_f t)/[1 + e^{-(t-t_{50})/\tau}])$, where I is the ThT intensity, t is time, and t_{50} is the time to half-maximal fluorescence intensity, and the remaining parameters are as described previously (*33*). In comparing the fibrillization kinetics under various experimental conditions, we used t_{50}, obtained directly from the fit to our data.

Determining r-IAPP Binding Free Energies. Free energies for the transfer of r-IAPP from water to lipid membranes were calculated using the relation $\Delta G = -RT \ln K_x$, where K_x represents the mole fraction partition coefficient (*34*). To determine K_x, r-IAPP was titrated with lipid membranes in the form of LUV (see Results for details). The measured ellipticity at 222 nm for each titration point was normalized to the value obtained in the absence of lipid, plotted as a function of the added lipid concentration, and fitted to the following binding isotherm:

$$\Theta_{obs,norm} = \frac{K_x[L]}{[W] + K_x[L]}(\Theta_{bound,norm} - 1) + 1$$

where $\Theta_{obs,norm}$ is the normalized measured ellipticity at 222 nm, $\Theta_{bound,norm}$ is the normalized ellipticity at complete binding, [L] is the lipid concentration, and [W] is the molar concentration of water (55.3 M), to obtain the mole fraction partition coefficient (*34*).

RESULTS

Kinetics of Human IAPP Aggregation Is Modulated by Membrane PS Content and Ionic Strength. First, we investigated the kinetics of h-IAPP aggregation in the presence of LUV containing various amounts of the negatively charged lipid PS. To measure the kinetics of h-IAPP aggregation, we monitored the real-time emission intensity of ThT, which is known to increase in the presence of amyloid fibril formation (*35*, *36*). In the absence of LUV, freshly dissolved IAPP in 10 mM phosphate buffer showed a sigmoidal increase in ThT intensity (Figure 1A, curve i). EM analysis confirmed the formation of predominantly fibrillar h-IAPP aggregates (also see below). In the presence of LUV containing PS, we observed increases in ThT signal intensity on a much shorter time scale (Figure 1A, curves ii−iv). To compare the kinetics of IAPP aggregation in both the presence and absence of LUV, we determined the time to half-maximal signal intensity, t_{50}, by fitting our data to a sigmoidal curve (see Experimental Procedures). In the absence of lipid, h-IAPP aggregation kinetics exhibited a t_{50} of ∼10−14 h. In contrast, LUV containing 1, 10, and 25 mol % PS caused a reduction in t_{50} values to ∼6, 1.6, and 0.4 h, respectively [Figure 1C, open circles]. Interestingly, in the presence of LUV containing 66 and 90 mol % PS, we observed a t_{50} value greater than that observed for LUV with 10 mol % PS. Thus, there appears to be an optimal PS concentration for acceleration of IAPP fibrillization.

To investigate the effect under more physiological ionic strength conditions, we also measured the aggregation kinetics of h-IAPP in buffer containing 100 mM NaCl. Also

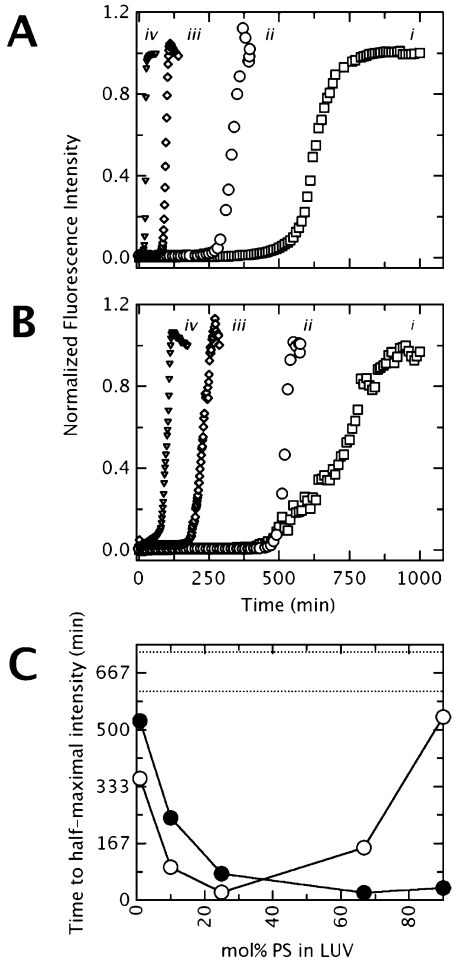

FIGURE 1: LUV-mediated modulation of the kinetics of IAPP aggregation. Wild-type human IAPP exhibited time-dependent increases in ThT fluorescence indicating the formation of aggregates. The kinetics of aggregate formation is modulated by the addition of LUV containing negatively charged phosphatidylserine (PS). Representative ThT emission curves for human IAPP in (A) 10 mM phosphate buffer and (B) 10 mM phosphate buffer with 100 mM NaCl. Curve i (in panels A and B) is in the absence of lipid membranes. Curves ii−iv (in panels A and B) represent ThT increases observed in the presence of LUV containing 1, 10, and 25 mol % PS, respectively. All ThT curves are shown renormalized on the basis of the maximum observed intensity at the end of each aggregation reaction. All measurements were taken with a peptide concentration of 25 μM, a lipid concentration of 500 μM, and a ThT concentration of 25 μM. For comparison of aggregation kinetics, we obtained the time to half-maximal signal intensity, t_{50}, by fitting each curve to a sigmoidal curve (see Experimental Procedures). (C) Values of t_{50} obtained in 10 mM phosphate buffer (○) and in 10 mM phosphate buffer with 100 mM NaCl (●) for human IAPP with LUV containing 1, 10, 25, 66, and 90 mol % PS. The dotted lines in panel C represent the t_{50} values obtained in the absence of LUV for 10 mM phosphate buffer (bottom) and buffer with 100 mM NaCl (top).

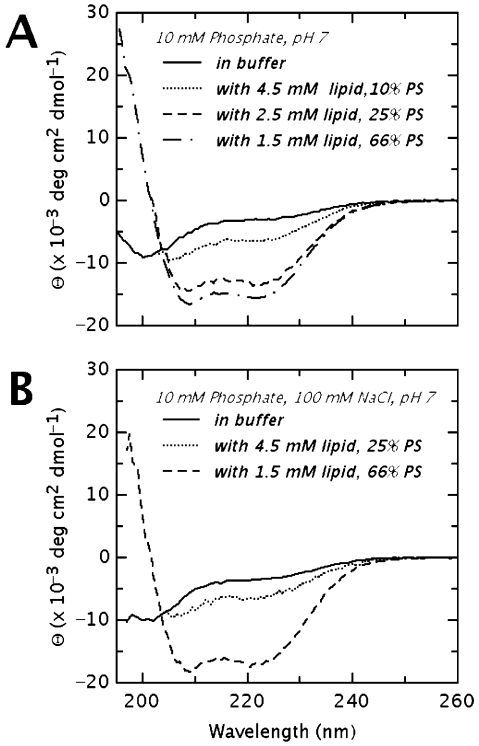

FIGURE 2: In the presence of membranes, IAPP adopts an α-helical conformation. Representative CD spectra obtained in (A) 10 mM phosphate buffer and (B) 10 mM phosphate buffer with 100 mM NaCl. Spectra obtained for IAPP in solution are indicative of an unordered backbone (—). Spectra obtained in the presence of 10 (•••), 25 (− − −), and 66 mol % PS (−•−) containing LUV exhibit the presence of two minima at 208 and 222 nm characteristic of an α-helical conformation. On the basis of the spectra in 66 mol % PS, which were collected under saturating binding conditions, the helicity of membrane-bound IAPP is estimated to be ∼42−50% (see the text for details). All spectra were recorded at a peptide concentration of 25 μM.

under these conditions, we found that IAPP aggregation is accelerated in the presence of LUV containing PS (Figure 1B, curves i−iv). Although the kinetics of aggregation followed a pattern similar to that observed in the absence of salt, acceleration was suppressed at low PS concentrations, and the optimal PS concentration was shifted to a higher value in the presence of salt [Figure 1C, filled circles]. At neutral pH, h-IAPP is positively charged (N-terminal charge, Lys 1, and Arg 11). Thus, electrostatic interactions could play a role in its interaction with negatively charged membranes. Consistent with this notion, it appears that the salt effect might, at least in part, be due to a shielding of electrostatic interaction between IAPP and the negatively charged membranes.

In the Presence of Lipid Membranes, Human IAPP Initially Adopts an α-Helical Conformation. Although IAPP−membrane interactions have been reported, the molecular details of this association have not been described. Here, we used CD spectroscopy to investigate the structure of h-IAPP in the presence of LUV. The CD spectrum of h-IAPP freshly dissolved in 10 mM phosphate buffer displays a peak with negative ellipticity at ∼198 nm (Figure 2A, black line) and is indicative of a predominantly unordered backbone structure. Spectra obtained immediately following the addition of LUV containing 10, 25, or 66 mol % PS displayed negative ellipticity at 208 and 222 nm (Figure 2A). These spectra are characteristic of an α-helical backbone structure. Similar spectra indicative of an α-helical conformation for h-IAPP were obtained with LUV in buffer containing 100 mM NaCl (Figure 2B). In general, an increased membrane PS concentration leads to an increased helicity. On the basis of CD spectra obtained with membranes containing 66 mol % PS under saturating binding conditions (i.e., where subsequent additions of LUV did not change the spectral intensity), it is possible to estimate the helicity of membrane-bound IAPP (see Experimental Procedures). Although this

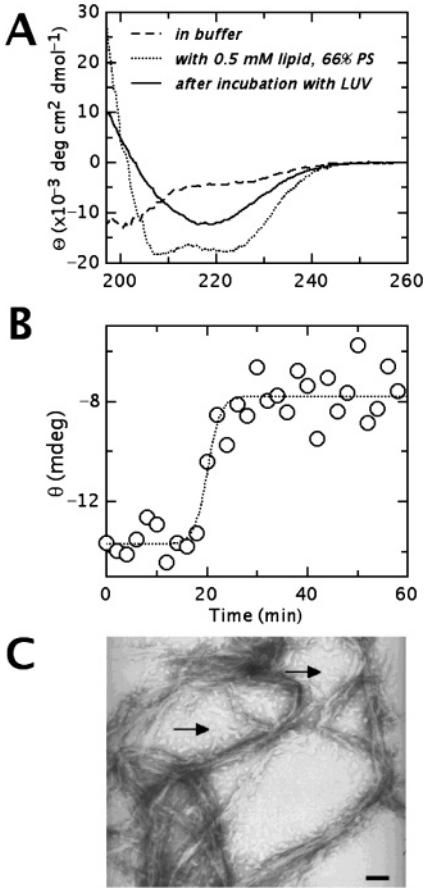

FIGURE 3: In the presence of membranes, IAPP undergoes an α-helix to β-sheet transition. (A) The CD spectrum obtained immediately after the addition of LUV containing 66 mol % PS is indicative of a helical conformation (•••). The spectrum obtained after incubation with LUV and an increase in ThT fluorescence intensity does not contain negative intensity at 208 nm and exhibits a minimum at 218 nm (—). The features are characteristic of a β-sheet conformation. (B) Disappearance of the helical form, in the presence of 66 mol % LUV in 10 mM phosphate buffer with 100 mM NaCl, as monitored by time-resolved CD spectral intensities at 208 nm, takes a sigmoidal form similar to our ThT data. (C) EM micrograph of IAPP aggregated in the presence of LUV containing 66 mol % PS showing the presence of fibrils with a diameter of ∼7 nm. These fibrils are similar in appearance to those formed in the absence of lipid membranes. Bar = 100 nm.

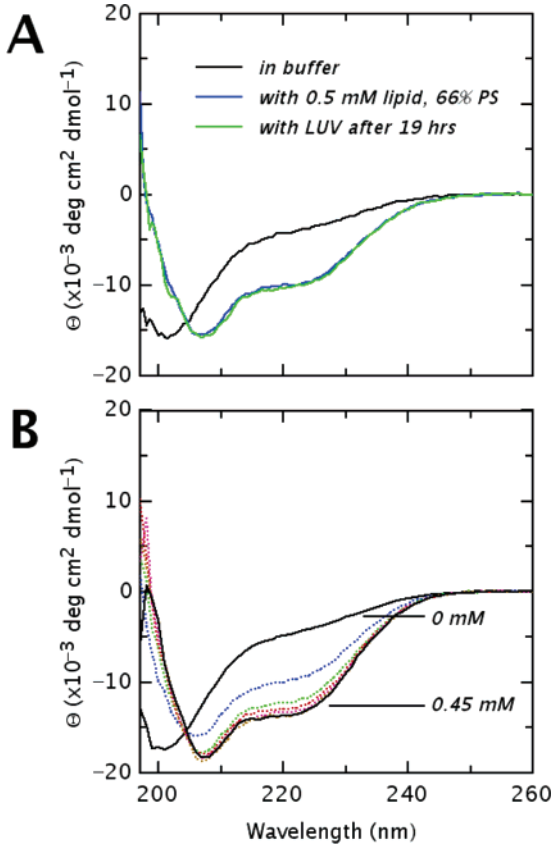

FIGURE 4: Rat IAPP adopts an α-helical conformation in the presence of lipid membranes. (A) The CD spectrum of r-IAPP in solution is indicative of an unordered backbone, and is similar to that of the human form (black line). Immediately upon the addition of LUV with 66 mol % PS, we obtain a spectrum characteristic of an α-helical conformation (blue line). Unlike in the case of human IAPP, rat IAPP remains helical even after prolonged exposure to membranes (green line). This observation is consistent with our ThT data for rat IAPP that do not show the formation of significant amounts of aggregates. (B) Successive addition of increasing amounts LUV to buffer containing rat IAPP gave rise to spectra with increasing α-helical content. We observe the presence of an isodichroic point at 204 nm indicating that binding of rat IAPP to the membrane is a two-state process, containing unordered peptide in solution and helical peptide bound to the membrane.

method is well established, the estimated helicity can vary due to uncertainties associated with setting the limiting values for completely helical and completely random coil structures (*37*). Using values for Θ_H of -34.7×10^3 deg cm^2 dmol^{-1} and for Θ_{RC} of 895 deg cm^2 dmol^{-1} at 222 nm, we estimate the helicity of membrane-bound IAPP to be ∼46−50%. If we use a Θ_{RC} of -1.5×10^3 deg cm^2 dmol^{-1}, based on CD spectra obtained in 6 M guanidine HCl (data not shown), where IAPP is expected to lack defined secondary structure, the helicity is calculated as ∼42−47%. Therefore, we estimate that ∼15−19 residues are in a helical conformation within membrane-bound IAPP. We observe that the helicity of IAPP in the strongly α-helix-promoting solvent HFIP is approximately 62−65% (or 23−24 residues, data not shown). The helicity of IAPP in the presence of membranes is in line with this upper limit of helicity obtained in HFIP.

Human IAPP Incubated with Lipid Membranes Undergoes a Conformational Rearrangement. To test for conformational changes upon membrane-dependent aggregation, we obtained CD spectra of h-IAPP after increases in ThT intensity had indicated the formation of aggregates (Figure 3A). These spectra, as illustrated for the representative case of h-IAPP in the presence of LUV containing 66 mol % PS (Figure 3A, solid line), contained a single peak with negative ellipticity at ∼218 nm, and are characteristic of a β-sheet conformation. Similar spectra were obtained for h-IAPP incubated with LUV containing other PS concentrations (data not shown). Time-resolved CD spectra obtained during the aggregation of IAPP in the presence of LUV containing 66 mol % PS indicate the conversion of the initial α-helical conformation to the final β-sheet form (data not shown). The loss of helicity, as measured by the intensity at 208 nm, exhibited a sigmoidal form similar to that of our ThT data (Figure 3B).

To further characterize the morphology of the LUV-catalyzed IAPP aggregates, we employed negative stain electron microscopy. Electron micrographs indicate the presence of mature fibrils with a diameter of ∼7 nm (Figure 3C), some of which are observed to be laterally aggregated into larger fibrillar assemblies. The morphology of fibrils

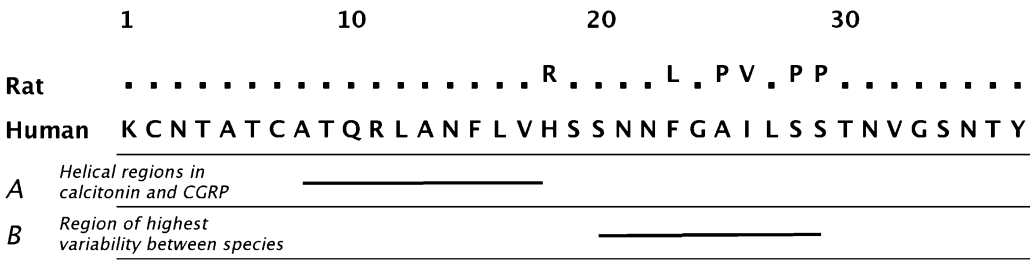

FIGURE 5: Sequence comparison of human and rat IAPP. The sequence of rat IAPP is significantly homologous (~84%) to that of the human form but does not form fibrils to a significant extent. The three proline residues in the C-terminal half of the rat IAPP are thought to play a key role in its inability to form fibrils. (A) Helical regions identified for calcitonin in SDS micells and the calcitonin gene-related peptide (CGRP) in a water/trifluoroethanol mixture. Calcitonin, CGRP, and IAPP are thought to belong to the CGRP superfamily of peptides, and therefore may contain similar helical regions. (B) Interspecies variation with regard to the ability to form fibrils has been attributed to residue differences within the region of residues 20−29.

formed in the presence of lipid membranes appears to be similar to that of fibrils formed from solutions of h-IAPP alone (*23*). In addition to the fibrillar structures, we observed the presence of spherical structures with a diameter between 17 and 33 nm (Figure 3C, arrow). These structures are too small to be LUV, which have a diameter of 100 nm. Although the exact nature of these spherical structures remains to be elucidated, they appear to be quite similar to nonfibrillar oligomers reported in the literature (*38*). However, at present, we cannot discount the possibility that these structures might also contain some lipids. In fact, a recent report suggests that lipids could become incorporated into IAPP aggregates (*39*).

Rat IAPP Adopts an α*-Helical Structure in the Presence of Lipid Membranes*. To determine the significance of the helical structure observed for IAPP in the presence of LUV, we investigated the conformation of rat IAPP in the presence of lipid membranes. The sequence of r-IAPP is significantly similar to that of the human form (~84%), differing by only six residues (Figure 5), but does not form significant amounts of amyloid fibrils (*40*). CD spectra of r-IAPP obtained in buffer (Figure 4A, black dotted line) are similar to those obtained for the human form and are indicative of a random conformation. As in the case of h-IAPP, the addition of LUV to r-IAPP induces an α-helical conformation (Figure 4A, black solid line). On the basis of the ellipticity at 222 nm, we estimate the α-helicity (see Experimental Procedures) of r-IAPP to be ~40% under conditions of saturating binding, which corresponds to ~15 residues in a helical conformation, suggesting that the membrane-bound structure of r-IAPP may be similar to that of its human counterpart. Although the CD spectra of h-IAPP and r-IAPP obtained in the presence of LUV are nearly identical, we observed a subtle difference. The r-IAPP spectrum exhibits a slightly more intense minimum at 208 nm, possibly indicating some contribution from a short polyproline II helix from the C-terminal proline rich region of r-IAPP.

In contrast to the case of h-IAPP, we did not observe a significant increase in ThT intensity upon incubation of r-IAPP with or without LUV (data not shown). Furthermore, we did not observe an α-helix to *β*-sheet transition upon incubation with LUV, and r-IAPP remained helical following incubation with lipid membranes (Figure 4A, green line). Under these conditions, r-IAPP retains its helical conformation even after prolonged exposure (duration of experiment, ~19 days) to LUV (data not shown). Our ThT and CD data for r-IAPP in the presence of LUV are consistent with the inability of this peptide to aggregate and efficiently form amyloid fibrils. Thus, the ability to form a helical membrane-bound conformation alone is not sufficient for aggregation in the presence of LUV.

To obtain the binding free energy for the association of r-IAPP with LUV, we obtained CD spectra of r-IAPP after successive additions of vesicles. Increasing amounts of LUV gave rise to CD spectra with increasing helical content until binding was saturated (Figure 4B). Binding of r-IAPP appears to be a two-state process, giving rise to an isodichroic point at ~204 nm. These two states are most likely unstructured peptide in solution and partially helical peptide bound to lipid membranes. On the basis of such CD titration data, we estimate the transfer free energy (see Experimental Procedures for details) of r-IAPP from water to the lipid membrane to be approximately −7 and −9 kcal/mol for membranes containing 25 and 66 mol % PS, respectively, in the absence of salt and approximately −8 kcal/mol for membranes containing 66 mol % PS in the presence of 100 mM NaCl. As pointed out above, this dependence on salt and negatively charged lipid concentration suggests that electrostatics play a role in the membrane interaction of IAPP. Attempts to determine the partition free energies of h-IAPP proved to be more challenging due to aggregation in the presence of LUV. However, given the high degree of sequence similarity and their similar helicity, partition free energies for r-IAPP are likely to serve as approximate estimates for h-IAPP.

DISCUSSION

In this study, we provide evidence that PS-containing membranes promote IAPP aggregation (Figure 1). This aggregation depends on the concentration of negatively charged PS as well as ionic strength. Studies involving rodent pancreatic islets indicate that PS comprises 4−14 mol % of the total phospholipid content (*41*). Although we obtained the strongest enhancement of IAPP aggregation kinetics with 25 and 66 mol % PS (without and with salt, respectively), we observed significant acceleration even in the presence of more physiologically significant concentrations (1 and 10 mol % PS). In the case of PS, the lipid is found more highly enriched on the cytoplasmic face of the cell membranes. In light of these observations, membrane-mediated aggregation of IAPP could, in principle, play a role in its toxicity, especially if, as has been reported (*42, 43*), IAPP aggregation occurs on the cytoplasimic side of cellular membranes.

We found that, after its initial exposure to membranes, IAPP adopts an α-helical conformation (Figure 2A,B). Such

an induction of secondary structure has been observed for peptides that interact with membranes, and is strongly coupled to the energetics of peptide partitioning to the membrane (*44*, *45*). What region of membrane-bound IAPP adopts a helical conformation? Although our data do not indicate the location of the helical region, some information can be obtained by inspecting the structure of homologous peptides. It is believed that IAPP belongs to the calcitonin gene peptide superfamily (*46*). The solution NMR structures of calcitonin in the presence of SDS micelles, and the related calcitonin gene-related peptide (CGRP) structure in a water/trifluoroethanol mixture, reveal the presence of helical regions between residues 9 and 16 and between residues 8 and 18, respectively (Figure 5A) (*47*, *48*). The helical region of IAPP may be similar, but probably slightly longer given our estimates of 15−19 residues participating in helix formation. If so, the helix would likely extend toward the C-terminus, since the N-terminus (residues 1−7) contains a disulfide bridge that would prevent helix formation. In agreement with these considerations, our modeling based on residue hydrophobicity (http://blanco.biomol.uci.edu/mpex, using a window size of 18 residues) suggests that residues 10−27 of IAPP would have the highest hydrophobicity ($\Delta G_{\text{water-to-bilayer}} = -6$ kcal/mol) and amphipathicity (hydrophobic moment, $\mu = 4.86$) in a membrane-bound helical conformation. In the case of r-IAPP and calcitonin, the presence of proline residues toward the C-terminus of the two peptides may act to prevent the formation of secondary structure in this region. This may be especially true in the case of r-IAPP, which contains three proline residues in close proximity (residues 25, 28, and 29) (*49*). However, the destabilizing effect of prolines on helix formation may not be as pronounced in a membrane environment as in soluble globular proteins (*50*, *51*).

Upon incubation of h-IAPP with lipid membranes, we observed that IAPP undergoes a conformational rearrangement to adopt a predominantly β-sheet structure (Figure 3A,B). Although using CD spectra of aggregate suspensions to quantify the β-sheet content should be done with caution, given the propensity for aggregates to settle out of solution, on the basis of our CD spectra (Figure 3A), we estimate that at least 60% (or ~22 residues) of the peptide aggregated in the presence of LUV is in a β-sheet conformation. This estimate is in keeping with the finding that nearly all residues outside the seven to eight N-terminal residues are involved in formation of the predominantly β-sheet rich core of the fibril (*23*). Since the helical region of IAPP also has to be outside the N-terminus, peptide aggregation in the presence of LUV must, therefore, involve conversion of this initial membrane-bound helical region to a β-sheet.

A number of factors could contribute to the lipid-induced IAPP aggregation observed here. In particular, it appears very likely that the partial helical structure anchors the peptide to the membrane surface. The resulting increased concentration of the peptide at the membrane surface, and the reduction in dimensionality, would facilitate the interaction of membrane-bound peptides leading to the formation of aggregates with β-sheet structure. Additional driving force for the aggregation could come from the favorable energy that would be gained by hydrogen bonding the backbone during the conversion of the membrane-bound unstructured region to a β-sheet (*52*). We do not observe aggregation of r-IAPP in the presence of LUV. Given that the most significant difference in primary structure between h-IAPP and r-IAPP lies within residues 25−29 (note the three proline residues in this region of r-IAPP), we expect this region to play a prominent role in the LUV-mediated aggregation process. Interestingly, interspecies variation with regard to IAPP amyloidogenicity has been attributed to residue variation within the region of residues 20−29 (Figure 5B). Regardless of the precise mechanism, two potential reasons for the observed decrease in the rate of acceleration of h-IAPP aggregation at high PS concentrations exist. First, this decrease in the rate of acceleration could be due to the reduction of free monomer in solution or, second, to a more stable helical form increasing the barrier to aggregation at high PS concentrations.

In summary, our study shows that IAPP aggregation is significantly modulated when associated with membranes containing PS. Our data serve to strengthen previous observations that anionic lipids play a key role in membrane-mediated IAPP fibril formation. Membrane-bound IAPP adopts an α-helical conformation yet undergoes a conformational change to a predominantly β-sheet form upon aggregation in the presence of lipid membranes. Our analysis of the data allows us to describe the membrane-mediated aggregation of IAPP in a structural context. Further studies should enable us to carry out a higher-resolution conformational analysis of membrane-bound IAPP that, in turn, will assist us in describing the mechanism of membrane-mediated IAPP aggregation.

ACKNOWLEDGMENT

We thank Diana Gegala for her assistance during the preparation of the manuscript.

REFERENCES

1. Soto, C. (2003) Unfolding the role of protein misfolding in neurodegenerative diseases, *Nat. Rev. Neurosci. 4*, 49−60.
2. Hull, R. L., Westermark, G. T., Westermark, P., and Kahn, S. E. (2004) Islet amyloid: A critical entity in the pathogenesis of type 2 diabetes, *J. Clin. Endocrinol. Metab. 89*, 3629−3643.
3. McLaurin, J., Franklin, T., Chakrabartty, A., and Fraser, P. E. (1998) Phosphatidylinositol and inositol involvement in Alzheimer amyloid-β fibril growth and arrest, *J. Mol. Biol. 278*, 183−194.
4. Matsuzaki, K., and Horikiri, C. (1999) Interactions of amyloid β-peptide (1−40) with ganglioside-containing membranes, *Biochemistry 38*, 4137−4142.
5. Pillot, T., Goethals, M., Vanloo, B., Talussot, C., Brasseur, R., Vandekerckhove, J., Rosseneu, M., and Lins, L. (1996) Fusogenic properties of the C-terminal domain of the Alzheimer β-amyloid peptide, *J. Biol. Chem. 271*, 28757−28765.
6. Kremer, J. J., Pallitto, M. M., Sklansky, D. J., and Murphy, R. M. (2000) Correlation of β-amyloid aggregate size and hydrophobicity with decreased bilayer fluidity of model membranes, *Biochemistry 39*, 10309−10318.
7. Mason, R. P., Jacob, R. F., Walter, M. F., Mason, P. E., Avdulov, N. A., Chochina, S. V., Igbavboa, U., and Wood, W. G. (1999) Distribution and fluidizing action of soluble and aggregated amyloid β-peptide in rat synaptic plasma membranes, *J. Biol. Chem. 274*, 18801−18807.
8. Yang, A. J., Chandswangbhuvana, D., Margol, L., and Glabe, C. G. (1998) Loss of endosomal/lysosomal membrane impermeability is an early event in amyloid Aβ1−42 pathogenesis, *J. Neurosci. Res. 52*, 691−698.
9. McLaurin, J., and Chakrabartty, A. (1996) Membrane disruption by Alzheimer β-amyloid peptides mediated through specific binding to either phospholipids or gangliosides. Implications for neurotoxicity, *J. Biol. Chem. 271*, 26482−26489.
10. Arispe, N., Pollard, H. B., and Rojas, E. (1993) Giant multilevel cation channels formed by Alzheimer disease amyloid β-protein

[Aβ P-(1−40)] in bilayer membranes, *Proc. Natl. Acad. Sci. U.S.A. 90*, 10573−10577.
11. Davidson, W. S., Jonas, A., Clayton, D. F., and George, J. M. (1998) Stabilization of α-synuclein secondary structure upon binding to synthetic membranes, *J. Biol. Chem. 273*, 9443−9449.
12. Volles, M. J., Lee, S. J., Rochet, J. C., Shtilerman, M. D., Ding, T. T., Kessler, J. C., and Lansbury, P. T., Jr. (2001) Vesicle permeabilization by protofibrillar α-synuclein: Implications for the pathogenesis and treatment of Parkinson's disease, *Biochemistry 40*, 7812−7819.
13. Kazlauskaite, J., Sanghera, N., Sylvester, I., Venien-Bryan, C., and Pinheiro, T. J. (2003) Structural changes of the prion protein in lipid membranes leading to aggregation and fibrillization, *Biochemistry 42*, 3295−3304.
14. Bokvist, M., Lindstrom, F., Watts, A., and Grobner, G. (2004) Two types of Alzheimer's β-amyloid (1−40) peptide membrane interactions: Aggregation preventing transmembrane anchoring versus accelerated surface fibril formation, *J. Mol. Biol. 335*, 1039−1049.
15. Lee, H. J., Choi, C., and Lee, S. J. (2002) Membrane-bound α-synuclein has a high aggregation propensity and the ability to seed the aggregation of the cytosolic form, *J. Biol. Chem. 277*, 671−678.
16. Perrin, R. J., Woods, W. S., Clayton, D. F., and George, J. M. (2001) Exposure to long chain polyunsaturated fatty acids triggers rapid multimerization of synucleins, *J. Biol. Chem. 276*, 41958−41962.
17. Necula, M., Chirita, C. N., and Kuret, J. (2003) Rapid anionic micelle-mediated α-synuclein fibrillization in vitro, *J. Biol. Chem. 278*, 46674−46680.
18. Chirita, C. N., Necula, M., and Kuret, J. (2003) Anionic micelles and vesicles induce tau fibrillization in vitro, *J. Biol. Chem. 278*, 25644−25650.
19. Kahn, S. E., Andrikopoulos, S., and Verchere, C. B. (1999) Islet amyloid: A long-recognized but underappreciated pathological feature of type 2 diabetes, *Diabetes 48*, 241−253.
20. Higham, C. E., Jaikaran, E. T., Fraser, P. E., Gross, M., and Clark, A. (2000) Preparation of synthetic human islet amyloid polypeptide (IAPP) in a stable conformation to enable study of conversion to amyloid-like fibrils, *FEBS Lett. 470*, 55−60.
21. Kayed, R., Bernhagen, J., Greenfield, N., Sweimeh, K., Brunner, H., Voelter, W., and Kapurniotu, A. (1999) Conformational transitions of islet amyloid polypeptide (IAPP) in amyloid formation in vitro, *J. Mol. Biol. 287*, 781−796.
22. Sumner Makin, O., and Serpell, L. C. (2004) Structural Characterisation of Islet Amyloid Polypeptide Fibrils, *J. Mol. Biol. 335*, 1279−1288.
23. Jayasinghe, S. A., and Langen, R. (2004) Identifying structural features of fibrillar islet amyloid polypeptide using site-directed spin labeling, *J. Biol. Chem. 279*, 48420−48425.
24. Torok, M., Milton, S., Kayed, R., Wu, P., McIntire, T., Glabe, C. G., and Langen, R. (2002) Structural and dynamic features of Alzheimer's Aβ peptide in amyloid fibrils studied by site-directed spin labeling, *J. Biol. Chem. 277*, 40810−40815.
25. Der-Sarkissian, A., Jao, C. C., Chen, J., and Langen, R. (2003) Structural organization of α-synuclein fibrils studied by site-directed spin labeling, *J. Biol. Chem. 278*, 37530−37535.
26. Margittai, M., and Langen, R. (2004) Template Assisted Filament Growth by Parallel Stacking of Tau, *Proc. Natl. Acad. Sci. U.S.A. 101*, 10278−10283.
27. Mirzabekov, T. A., Lin, M. C., and Kagan, B. L. (1996) Pore formation by the cytotoxic islet amyloid peptide amylin, *J. Biol. Chem. 271*, 1988−1992.
28. Kurganov, B., Doh, M., and Arispe, N. (2004) Aggregation of liposomes induced by the toxic peptides Alzheimer's Aβs, human amylin and prion (106−126): Facilitation by membrane-bound GM1 ganglioside, *Peptides 25*, 217−232.
29. Anguiano, M., Nowak, R. J., and Lansbury, P. T., Jr. (2002) Protofibrillar islet amyloid polypeptide permeabilizes synthetic vesicles by a pore-like mechanism that may be relevant to type II diabetes, *Biochemistry 41*, 11338−11343.
30. Knight, J. D., and Miranker, A. D. (2004) Phospholipid catalysis of diabetic amyloid assembly, *J. Mol. Biol. 341*, 1175−1187.
31. Luo, P., and Baldwin, R. L. (1997) Mechanism of helix induction by trifluoroethanol: A framework for extrapolating the helix-forming properties of peptides from trifluoroethanol/water mixtures back to water, *Biochemistry 36*, 8413−8421.
32. Rohl, C. A., and Baldwin, R. L. (1997) Comparison of NH exchange and circular dichroism as techniques for measuring the parameters of the helix-coil transition in peptides, *Biochemistry 36*, 8435−8442.
33. Nielsen, L., Khurana, R., Coats, A., Frokjaer, S., Brange, J., Vyas, S., Uversky, V. N., and Fink, A. L. (2001) Effect of environmental factors on the kinetics of insulin fibril formation: Elucidation of the molecular mechanism, *Biochemistry 40*, 6036−6046.
34. White, S. H., Wimley, W. C., Ladokhin, A. S., and Hristova, K. (1998) Protein folding in membranes: Determining energetics of peptide-bilayer interactions, *Methods Enzymol. 295*, 62−87.
35. Kudva, Y. C., Mueske, C., Butler, P. C., and Eberhardt, N. L. (1998) A novel assay in vitro of human islet amyloid polypeptide amyloidogenesis and effects of insulin secretory vesicle peptides on amyloid formation, *Biochem. J. 331*, 809−813.
36. Naiki, H., Higuchi, K., Hosokawa, M., and Takeda, T. (1989) Fluorometric determination of amyloid fibrils in vitro using the fluorescent dye, thioflavin T1, *Anal. Biochem. 177*, 244−249.
37. Ladokhin, A. S., and White, S. H. (1999) Folding of amphipathic α-helices on membranes: Energetics of helix formation by melittin, *J. Mol. Biol. 285*, 1363−1369.
38. Kayed, R., Sokolov, Y., Edmonds, B., McIntire, T. M., Milton, S. C., Hall, J. E., and Glabe, C. G. (2004) Permeabilization of lipid bilayers is a common conformation-dependent activity of soluble amyloid oligomers in protein misfolding diseases, *J. Biol. Chem. 279*, 46363−46366.
39. Sparr, E., Engel, M. F., Sakharov, D. V., Sprong, M., Jacobs, J., de Kruijff, B., Hoppener, J. W., and Killian, J. A. (2004) Islet amyloid polypeptide-induced membrane leakage involves uptake of lipids by forming amyloid fibers, *FEBS Lett. 577*, 117−120.
40. Green, J., Goldsbury, C., Mini, T., Sunderji, S., Frey, P., Kistler, J., Cooper, G., and Aebi, U. (2003) Full-length rat amylin forms fibrils following substitution of single residues from human amylin, *J. Mol. Biol. 326*, 1147−1156.
41. Rustenbeck, I., Matthies, A., and Lenzen, S. (1994) Lipid composition of glucose-stimulated pancreatic islets and insulin-secreting tumor cells, *Lipids 29*, 685−692.
42. Janson, J., Soeller, W. C., Roche, P. C., Nelson, R. T., Torchia, A. J., Kreutter, D. K., and Butler, P. C. (1996) Spontaneous diabetes mellitus in transgenic mice expressing human islet amyloid polypeptide, *Proc. Natl. Acad. Sci. U.S.A. 93*, 7283−7288.
43. O'Brien, T. D., Butler, P. C., Kreutter, D. K., Kane, L. A., and Eberhardt, N. L. (1995) Human islet amyloid polypeptide expression in COS-1 cells. A model of intracellular amyloidogenesis, *Am. J. Pathol. 147*, 609−616.
44. White, S. H., and Wimley, W. C. (1999) Membrane protein folding and stability: Physical principles, *Annu. Rev. Biophys. Biomol. Struct. 28*, 319−365.
45. Kaiser, E. T., and Kezdy, F. J. (1983) Secondary structures of proteins and peptides in amphiphilic environments (A review), *Proc. Natl. Acad. Sci. U.S.A. 80*, 1137−1143.
46. Wimalawansa, S. J. (1997) Amylin, calcitonin gene-related peptide, calcitonin, and adrenomedullin: A peptide superfamily, *Crit. Rev. Neurobiol. 11*, 167−239.
47. Motta, A., Andreotti, G., Amodeo, P., Strazzullo, G., and Castiglione Morelli, M. A. (1998) Solution structure of human calcitonin in membrane-mimetic environment: The role of the amphipathic helix, *Proteins 32*, 314−323.
48. Breeze, A. L., Harvey, T. S., Bazzo, R., and Campbell, I. D. (1991) Solution structure of human calcitonin gene-related peptide by ^{1}H NMR and distance geometry with restrained molecular dynamics, *Biochemistry 30*, 575−582.
49. Balali-Mood, K., Ashley, R. H., Hauss, T., and Bradshaw, J. P. (2005) Neutron diffraction reveals sequence-specific membrane insertion of pre-fibrillar islet amyloid polypeptide and inhibition by rifampicin, *FEBS Lett. 579*, 1143−1148.
50. Li, S. C., Goto, N. K., Williams, K. A., and Deber, C. M. (1996) α-Helical, but not β-sheet, propensity of proline is determined by peptide environment, *Proc. Natl. Acad. Sci. U.S.A. 93*, 6676−6681.
51. Liu, L. P., and Deber, C. M. (1998) Uncoupling hydrophobicity and helicity in transmembrane segments. α-Helical propensities of the amino acids in non-polar environments, *J. Biol. Chem. 273*, 23645−23648.
52. Wimley, W. C., Hristova, K., Ladokhin, A. S., Silvestro, L., Axelsen, P. H., and White, S. H. (1998) Folding of β-sheet membrane proteins: A hydrophobic hexapeptide model, *J. Mol. Biol. 277*, 1091−1110.

BI050840W